SAGE Publishing

Research Article

Adsorption-Oxidation Mechanism of δ-MnO$_2$ to Remove Methylene Blue

Ge Yan [ID],[1] **Pu Wang** [ID],[2] **Yuqian Li** [ID],[1] **Zhangjie Qin** [ID],[1] **Shuai Lan** [ID],[1] **Yupeng Yan** [ID],[1] **Qin Zhang** [ID],[1] **and Xiaodi Cheng** [ID][1]

[1]*Key Laboratory of Poyang Lake Watershed Agricultural Resources and Ecology of Jiangxi Province, College of Land Resources and Environment, Jiangxi Agricultural University, Nanchang 330045, China*
[2]*Wuhan Institute of Landscape Architecture, Wuhan 430081, China*

Correspondence should be addressed to Xiaodi Cheng; 305805978@qq.com

The material, δ-MnO$_2$, has exhibited superior performance on the removal of methylene blue (MB), but the process is significantly impacted by pH, and the impacting mechanism is still unclear. In this study, the effects of pH on the removal mechanism of MB using synthesized δ-MnO$_2$ were investigated by distinguishing the adsorption and oxidation of MB by δ-MnO$_2$ during the removal process in the dark. The results show that the total removal efficiency of MB by δ-MnO$_2$ decreased significantly with an increase in the pH. MB could be removed by δ-MnO$_2$ via an adsorption mechanism and oxidation mechanism, and the proportion of adsorptive removal and oxidative removal was different under different pH conditions. With an increase in the initial pH from 2.00 to 8.05, the redox potential of δ-MnO$_2$ decreased, and its oxidation ability for the removal of MB also gradually decreased. In contrast, the surface negative charges of δ-MnO$_2$ increased with an increase in the pH, and the adsorption ability towards positively charged MB also gradually increased. This indicates that the effects of pH on the removal of MB by δ-MnO$_2$ are primarily dominated by its influence on the oxidation ability of δ-MnO$_2$. In addition, it is further proved that the pH value has a significant effect on the oxidation and adsorption of MB on δ-MnO$_2$. Moreover, the significant effects of pH on the oxidation of MB by δ-MnO$_2$ are further demonstrated by observing the changes in Mn^{2+} and the UV-Vis spectra of intermediate products during the reaction, as well as the changes in the FTIR and XPS characterizations of δ-MnO$_2$ after the reaction.

1. Introduction

Manganese oxides widely exist in the earth's surface and water environments, and they are important components of soil and sediment [1]. In the microstructures of manganese oxides, manganese atoms coordinate with oxygen atoms in the form of [MnO$_6$] octahedra, and the [MnO$_6$] octahedra form single chains through coedge connections. These single chains are connected by sharing edges or corner oxygen atoms forming manganese oxides with different crystal structures [2]. The surface of manganese oxides belongs to hydrated oxide types with variable surface charges [3]. Because the zero point of charge (ZPC) of manganese oxides is very low, they are usually negatively charged within the normal pH range, which can adsorb charged heavy metal ions or organic pollutants [4–6]. Manganese oxides are primarily composed of high valent Mn(III) and Mn(IV) [7], which have high redox potentials. Hence, the removal towards organic pollutants can be achieved via oxidation reactions [8–10]. As a semiconductor, manganese oxides also exhibit photocatalytic activity, which can photocatalytically remove organic pollutants by irradiation [11]. Manganese oxides are often used to remove organic pollutants due to their multiple environmental properties, such as adsorption, oxidation, and photocatalysis [12, 13].

More than 7×10^5 tons of dyes and pigments widely used in many industries are produced every year, of which more than 10% are found in wastewater [14]. MB has a high chroma, and it is difficult to remove biologically [15]. It has been widely studied as a representative dye because it is a

serious environmental pollutant [16]. A large number of studies have shown that manganese oxides can effectively remove MB, but the efficiency is significantly affected by pH [17–19]. A study by Kuan et al. in 2011 showed that the removal capacity of γ-MnO$_2$ towards MB at pH 7.2 was lower than that at pH 4.8. By measuring the total organic carbon (TOC) of the reactants, it was speculated that there was an oxidative removal mechanism in the removal process of MB by γ-MnO$_2$ [20]. Kuan et al. subsequently found that pyrolusite could oxidatively remove MB when the pH was lower than its pH$_{iep}$ (4.70), while when the pH was higher than its pH$_{iep}$ (4.70), cationic MB was more easily adsorbed on pyrolusite electrostatically [21]. In 2017, Peng et al. used MnO$_2$ nanosheets to remove MB, and it was found that the removal efficiency gradually decreased with an increase in pH from 2 to pH$_{zpc}$3.69, while the removal efficiency gradually increased when the pH increased from pH$_{zpc}$3.69 to 12. They speculated that the effective removal observed at pH $<$ pH$_{zpc}$3.69 was due to the oxidation of MB by MnO$_2$ nanosheets, while at pH $>$ pH$_{zpc}$3.69, the removal was due to the electrostatic adsorption of MB by MnO$_2$ nanosheets [22]. Wang et al. found that with an increase in pH from 3.0 to 9.0, the total removal efficiency of MB decreased from 99.3% to 84.7%, and the oxidative removal efficiency decreased from 98.7% to 43.0%, while the adsorptive removal efficiency increased from 0.6% to 41.7% [18]. The above studies indicated that there existed two possible mechanisms for the removal of MB by manganese oxides: (1) MB with positive charges can be adsorbed on the surface of manganese oxides due to the large number of negative charges on the surface and (2) manganese oxides can remove MB via oxidation reactions due to their high redox potential. The surface charges and redox potentials of manganese oxide are impacted by pH. It is unclear how such an impact affects the adsorption or oxidation of MB by manganese oxides and whether there is a coupling mechanism between the two degradation mechanisms. In addition, all the above studies were conducted under light, and the photocatalytic degradation of MB by manganese oxides was not considered.

Therefore, in this study, the common manganese oxide, δ-MnO$_2$, was selected as a representative for manganese oxides. The effects of pH on the removal mechanism of MB by δ-MnO$_2$ were studied by analyzing the adsorption amount and oxidation amount of MB by δ-MnO$_2$, as well as the changes in pH, Mn^{2+}, and products during the reaction process. The reaction was conducted in the dark in order to avoid the photocatalytic effect of δ-MnO$_2$.

2. Materials and Methods

2.1. Synthesis and Characterization.
The used δ-MnO$_2$ were prepared with KMnO$_4$ and HCl, typically in a triangular flask with 300-400 mL of deionized water boiled in a constant temperature oil bath (110°C). Then, 120 mL of 6 mol/L HCl was added dropwise at a rate of 0.7 mL/min under strong stirring. After the addition was completed, the reaction was continued for 30 min, and the obtained product was aged at 60°C for 12 h [23]. After washing with deionized water to conductivity of $<$15 μs/cm, the final product was

dried in a 40°C oven, ground and passed through a 60-mesh sieve, and then placed in a desiccator for later use. Methylene blue (**purity $>$ 98**%) was purchased from Beijing Guangcheng Chemical Reagent Co. Ltd., China, and used without further purification. All other employed chemicals are of analytical reagent grade. The chemical structure of MB was given previously.

2.2. Characterization.
The crystal structure of the sample was determined by the Bruker Advance D8 X-ray powder diffraction (XRD) with CuKα radiation at 40 kV tube voltage, 40 mA tube current, 1°/min scanning speed, scanning interval of 5°-85°, and step size of 0.02°. The morphology of δ-MnO$_2$ was observed under the scanning electron microscope (SEM) of FEI Nova NanoSEM450. Transmission electron microscope (TEM) analysis was used to analyze the morphology and particle size characteristics by JEOL JEM-2100. The specific surface area (SSA) was determined using Quantachrome Autosorb-1. The zero point of charge (ZPC) was measured by the rapid potentiometric titration method. The average oxidation state (AOS) of Mn was measured by the oxalic acid-permanganate back-titration method [24].

2.3. Dye Removal

2.3.1. Kinetic.
100 mL 160 μmol/L dye solution (pH 3.99) was added into 100 mL 400 mg/L δ-MnO$_2$ suspension (pH 4.00) in a 250 mL triangle bottle under magnetic stirring, and the tin paper was wrapped in a triangular bottle to avoid light. The pH of dye and δ-MnO$_2$ was adjusted with HCl or NaOH solution until the pH value is stable in ±0.05 in 12 h. 10 mL of the supernatant was sampled using a syringe and immediately filtered through a 0.45 μm membrane filter at 0 min, 1 min, 3 min, 5 min, 9 min, 15 min, 20 min, 30 min, 60 min, 90 min, 180 min, and 240 min, respectively. In addition, two parallel experiments were set. The liquid under test was ally determined by the UV spectrophotometer (UV). The removal rate R, q_e of dye was calculated by

$$R = \frac{c_0 - c_t}{C_0} \times 100\%, \tag{1}$$

$$q_e = \frac{(c_0 - c_e)}{W} \times v, \tag{2}$$

where c_0 (μmol/L), c_t (μmol/L), and c_e (μmol/L) are the initial concentrations, dye concentration at contact time (t), and dye concentration at equilibrium, respectively. It is used to evaluate the degree of removal. W and V represent adsorbent dosage (mg) and dye solution volume (L), respectively. Then, fitting was obtained using the experimental kinetic data with the linear forms of the two kinetic models: the pseudo-first-order (PFO) and pseudo-second-order (PSO) models [25]; the specific formula is as follows:

$$\text{PFO} : \text{In}(Q_e - Q_t) = InQ_e - k_1 t, \tag{3}$$

$$\text{PSO} : \frac{t}{Q_t} = + \frac{t}{Q_e}, \tag{4}$$

TABLE 1: The physicochemical properties of δ-MnO$_2$.

Sample	S_{BET} (m^2/g)[a]	S_{μ} (m^2/g)[b]	S_{ext} (m^2/g)[c]	$V_{\mu p}$ (cm^3/g)[d]	AOS_{Mn}[e]	Composition	pH_{ZPC}[f]
δ-MnO$_2$	89.8	13.9	75.9	0.042	3.86	K$_{0.21}$MnO$_{2.03}$(H$_2$O)$_{0.71}$	1.78

[a]BET surface area; [b]micropore surface area; [c]external surface area; [d]micropore volume obtained from t-plots; [e]manganese average oxidation state; [f]zero point charge.
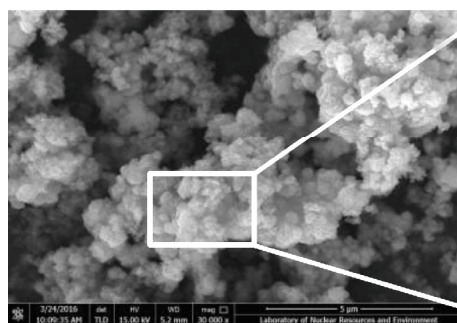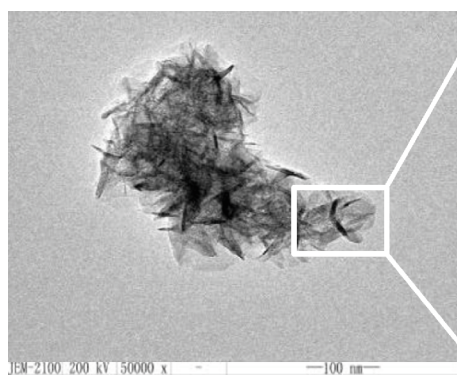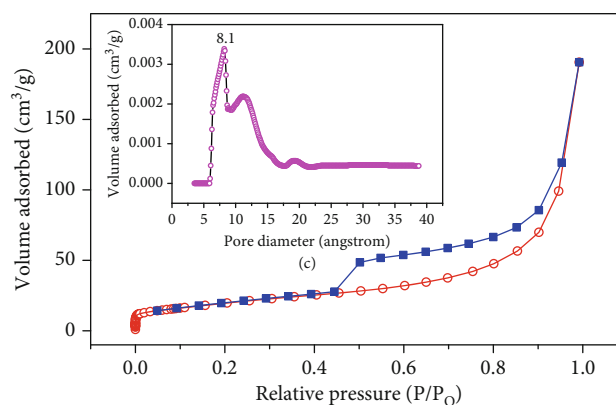

(a)

(b)

(d)

(e)

(f)

(g)
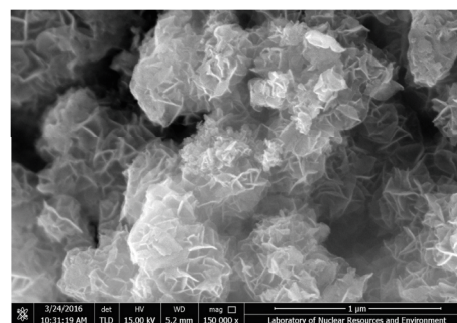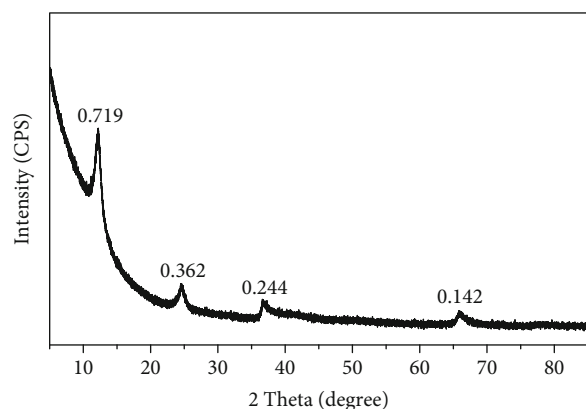
FIGURE 1: The XRD pattern (a) of δ-MnO$_2$; the N$_2$ adsorption/desorption isothermal plot of δ-MnO$_2$ (b) and the microspore size distribution plot (c) by the SF method; HRTEM (d, e) and HRSEM (f, g) images of δ-MnO$_2$.
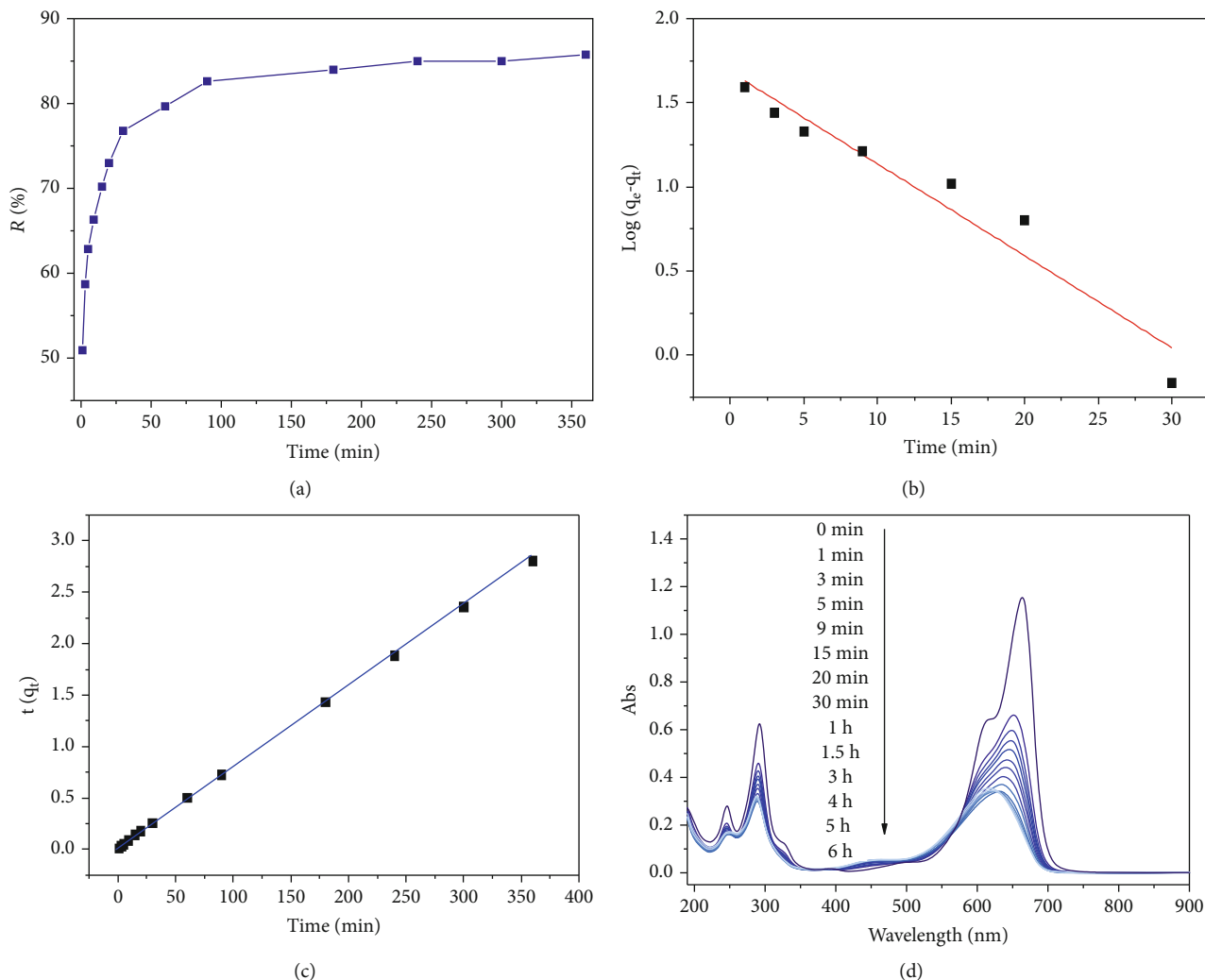
(a)

(b)

(c)

(d)

Figure 2: (a) Adsorption capacity as a function of contact time using the (b) pseudo-first-order, (c) pseudo-second-order, and (d) UV-Vis wavelength scan of MB dye.

where Q_e (mg/g) are adsorption capacity at equilibrium, Q_t (mg/g) are adsorption amount at contact time t (min), and k_1 and k_2 (min^{-1}) are first-order and second-order rate constants.

2.3.2. Removal Mechanism.

For the investigation of the mechanism, 50 mL of an 80 μmol/L MB solution was added into 50 mL of 200 mg/L δ-MnO$_2$ suspension in a 150 mL triangle bottle using tin foil to avoid light under magnetic stirring. The pH of the dye and the δ-MnO$_2$ was adjusted to the desired value (pH of 2.00, 4.01, 5.92, and 8.05) with the HCl or NaOH solution. The sampling times were 0.5 h, 1 h, and 3 h. At the specified time, 10 mL of the solution was filtered through a 0.45 μm membrane filter, and the removal efficiency was measured using the dye (Equation (1)) of the filter membrane as the total removal efficiency (R_T). Concurrently, another 10 mL solution was added using 2 mL of 20 g/L hydroxylamine hydrochloride (HONH$_3$Cl) and adding HONH$_3$Cl to dissolve the δ-MnO$_2$, releasing the dye adsorbed on the surface of the δ-MnO$_2$. The removal

Table 2: Parameters of the PFO and PSO kinetic models for the adsorption of MB on δ-MnO$_2$.

Kinetic model	q_{exp} (mg/g)	$q_{e,cal}$ (mg/g)	k (min^{-1})	R^2
PFO model	128.2	48.3	0.1259	0.9269
PSO model	128.2	128.5	0.0022	0.9999

ratio obtained by adding HONH$_3$Cl was the oxidative removal efficiency (R_{oxi}). The adsorptive removal efficiency (R_{ads}) was the difference between R_T and R_{oxi}. Each group was divided into two parallel groups.

The δ-MnO$_2$ that passed through the filter in the experiment was collected and repeatedly rinsed with ultrapure water and drying. The reacted δ-MnO$_2$ was subjected to FTIR and XPS measurement and compared with the initial δ-MnO$_2$ [26, 27]. UV-visible spectroscopy was utilized to determine dye removal efficiency and adsorption capacity. pH and the contents of Mn^{2+} of the solution after filtering the solution were also measured using atomic absorption
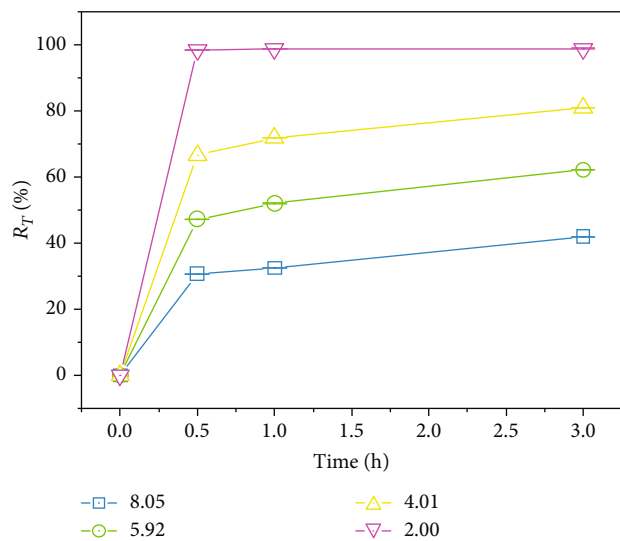
(a)
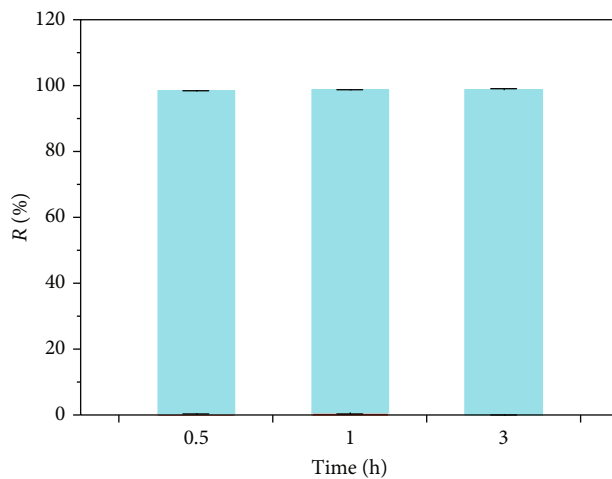
(b)
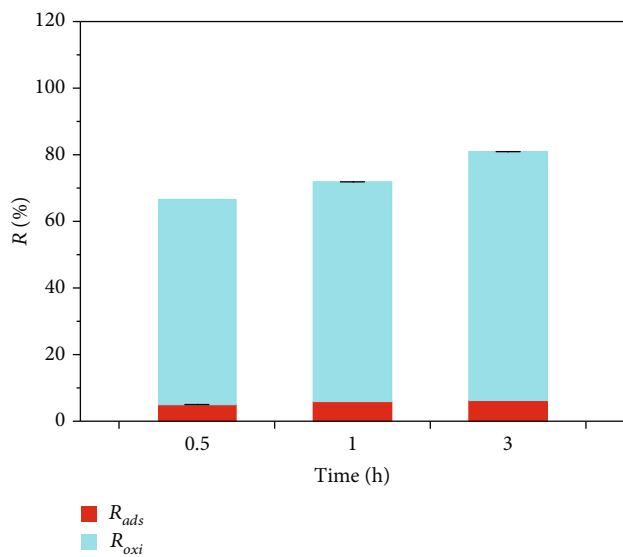
(c)

(d)

Figure 3: Continued.

(e)

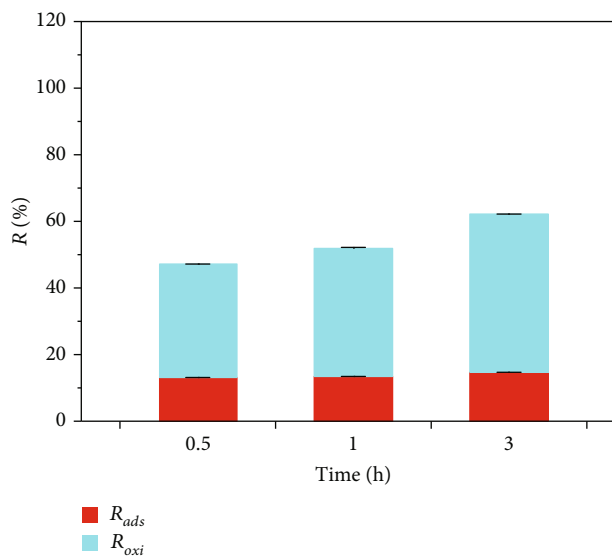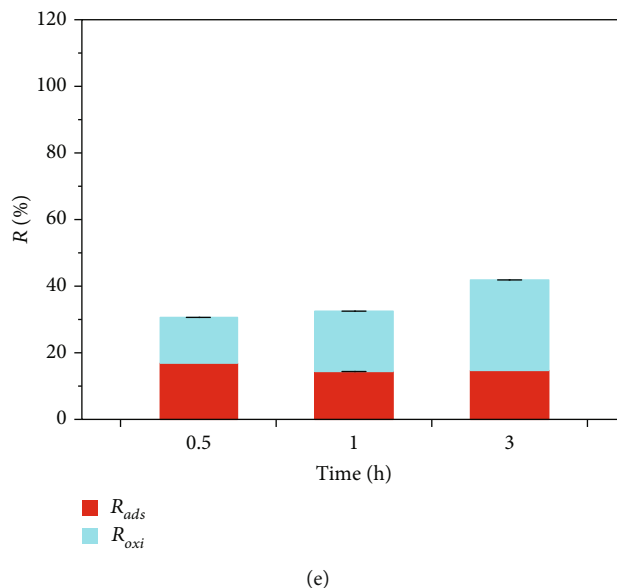FIGURE 3: Effect of pH on R_T (%) of MB (a); R_{ads} and R_{oxi} of MB in δ-MnO$_2$ at 0.5 h, 1 h, and 3 h, under the conditions of pH 2.00 (b), 4.01 (c), 5.92 (d), and 8.05 (e).

spectrometry (AAS, PerkinElmer AA900). All the experiments were run in duplicate, and the data presented are averages of this duplicate analysis.

3. Results

3.1. Characterization of δ-MnO$_2$. Table 1 shows the physicochemical properties of the as-synthesized δ-MnO$_2$. The powder XRD pattern of the as-synthesized sample is shown in Figure 1(a). The d values of the diffraction peaks of the as-synthesized sample were 0.719 nm, 0.362 nm, 0.244 nm, and 0.142 nm, which were consistent with the characteristic diffraction peaks of δ-MnO$_2$ (JCPDS 86-0666). Therefore, it was concluded that the as-synthesized sample was δ-MnO$_2$. Figure 1(b) shows the N$_2$ isothermal adsorption-desorption curve of δ-MnO$_2$ and the pore size distribution found using the Saito-Foley (SF) method. The measured N$_2$ isothermal adsorption-desorption curve was fitted using the Brunauer-Emmett-Teller (BET) method. The specific surface area of δ-MnO$_2$ was 89.8 m^2/g. The diameter of the micropores (Figure 1(c)) of δ-MnO$_2$ primarily distributed near 8.1 Å was fitted using the SF method. In addition, the micropore volume was 0.042 cm^3/g as analyzed using the total pore volume method. The micropore area and the external surface area of δ-MnO$_2$ were 13.9 m^2/g and 75.9 m^2/g (Table 1), respectively, as analyzed using the T-method. This indicates that the mesoporous specific surface area was much larger than the microporous specific surface area, meaning the mesoporous structure was dominant, although there existed a microporous structure in the as-synthesized δ-MnO$_2$. The SEM and TEM images of the as-synthesized δ-MnO$_2$ are shown in Figures 1(d)–1(g). Thin sheets of δ-MnO$_2$ were observed in the SEM images, and the TEM images further proved that the sample was composed of many thin sheet crystals aggregated to form

flower-like aggregates between one hundred and several hundreds of nanometers.

3.2. Kinetics of the Removal of MB by δ-MnO$_2$. The kinetics of the removal of MB by δ-MnO$_2$ are shown in Figure 2. The removal rate of MB was high within the initial 60 min, and the removal efficiency reached 50.93% at 1 min and 79.66% at 60 min. With an increase in the reaction time, the removal rate gradually decreased reaching equilibrium, and the removal efficiency was 85.74% (Figure 2(a)) after 6 h of reaction. The obtained kinetic data were linearly fitted using the pseudo-first-order (PFO) and the pseudo-second-order (PSO) kinetic models (Figures 2(b) and 2(c)). The fitting results are shown in Table 2. The correlation coefficients, R^2, of the PFO kinetics and PSO kinetics were 0.9269 and 0.9999, respectively, which indicated that the removal process of MB by δ-MnO$_2$ was more consistent with the second-order kinetics (Table 2). Figure 2(d) presents the UV-Vis wavelength scan of the reaction solution in the kinetic experiment. A blue shift was observed for the maximum absorption peak of MB in the full-band scan spectrum after reacting with δ-MnO$_2$.

3.3. The Effect of pH on Removal of MB. The changes in R_T, R_{oxi}, and R_{ads} of the MB by δ-MnO$_2$ at different pH are shown in Figure 3. With an increase in the initial pH, R_T of MB by δ-MnO$_2$ decreased gradually. After 0.5 h of reaction, R_T of MB by δ-MnO$_2$ was 98.38%, 66.66%, 47.22%, and 30.66% at pH of 2.00, 4.01, 5.92, and 8.05, respectively (Figure 3(a)). Thereafter, the reaction rate decreased, and the corresponding total removal efficiencies were 98.85%, 81.03%, 62.15%, and 41.91%, respectively, at 3 h of reaction (Figure 3(a)). For further analysis of the oxidation removal rate and adsorption removal rate of MB by δ-MnO$_2$, the law is as follows: the oxidation removal of MB by δ-MnO$_2$ has a similar change trend with the total removal rate, which
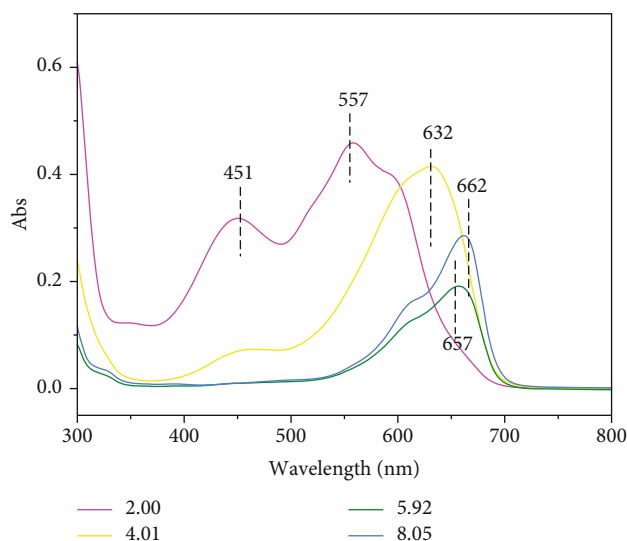
FIGURE 4: UV-Vis of MB after 3 hours of reaction at pH 2.00, 4.01 (dilute five times), 5.92 (dilute ten times), and 8.05 (dilute ten times).

FIGURE 5: Trend of the release of Mn^{2+} during the reaction in different pH.

gradually decreases from 98.85% to 27.29% as the pH increases. However, the adsorption removal rate of δ-MnO_2 on MB increased with the increase of the initial pH. When the pH increased from 2.00 to 4.01, 5.92, and 8.05, after 3 hours of reaction, the adsorption and removal rates of δ-MnO_2 on MB were 0%, 6.24%, 14.72%, and 14.62%, respectively.

The above results indicate that there was almost no adsorption of MB on the surface of δ-MnO_2 when the pH was 2.00 (Figure 3(b)), at which time, the removal of MB on the surface of δ-MnO_2 was primarily dominated by oxidation reactions. In addition, there was almost no MB in the reaction system. At a pH $\geq$ 4.01, the adsorption of MB by δ-MnO_2 increased to equilibrium, while the oxidative removal efficiency decreased (Figures 3(c)–3(e)).

4. Discussion

The above results show that the removal of MB by δ-MnO_2 includes oxidation removal and adsorption removal. In order to further explore the oxidation removal mechanism, the UV-visible spectra of the MB solution after reaction with δ-MnO_2 under different pH conditions are compared (Figure 4). The change of Mn^{2+} in the solution (Figure 5), FTIR spectrum (Figure 6), and XPS (Figure 7).

4.1. Oxidating MB by δ-MnO_2. In order to prove that the oxidation-reduction reaction occurred when δ-MnO_2 removes MB, the intermediate and final products of the oxidation reaction can be analyzed. First of all, it can be seen from Figure 4 that under the reaction conditions of different pH, the absorption peaks of the UV-Vis of the solution after the reaction are significantly different. With the decrease of pH, the absorption peak of the solution after the reaction changes significantly and accompanied by the appearance of new absorption peaks, such as absorption peaks at 451,
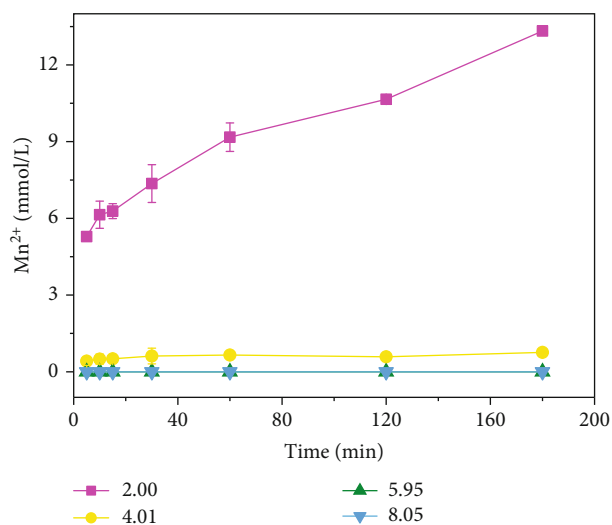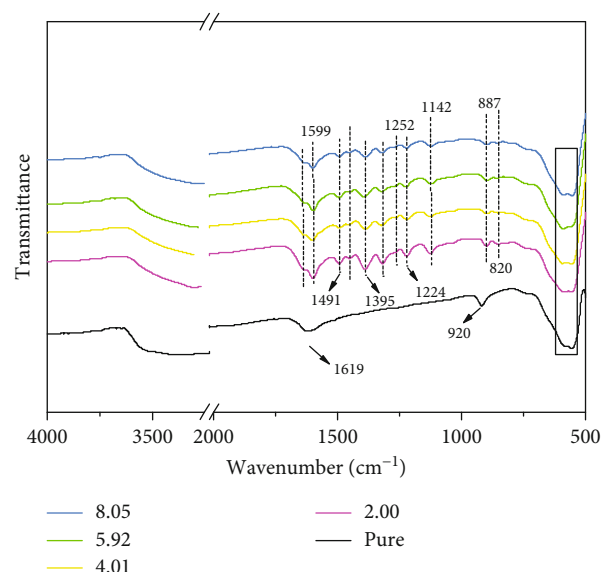

FIGURE 6: FTIR spectra of acid δ-MnO_2 (pure) and acid δ-MnO_2 after reaction with MB at different pH (2.00, 4.01, 5.92, and 8.05).

557, 608, 632, and 657 nm. And similar to the trend reported by Zaied et al., the MB removal process will produce intermediate products such as Azure B, Azure A, Azure C, and Thionin [28], and the absorption peak gradually shifts to the left. Therefore, it can be inferred that the oxidation-reduction reaction of MB occurred during the removal of δ-MnO_2, and as the pH of the reaction system gradually decreased, the oxidation capacity of δ-MnO_2 gradually increased, and the degradation degree of MB also increased, and intermediate products were formed. The maximum absorption peak also gradually shifted to the left.

By detecting the change of Mn^{2+} in the solution after the reaction, it can also be proved that the process of removing MB by δ-MnO_2 has undergone an oxidation-reduction
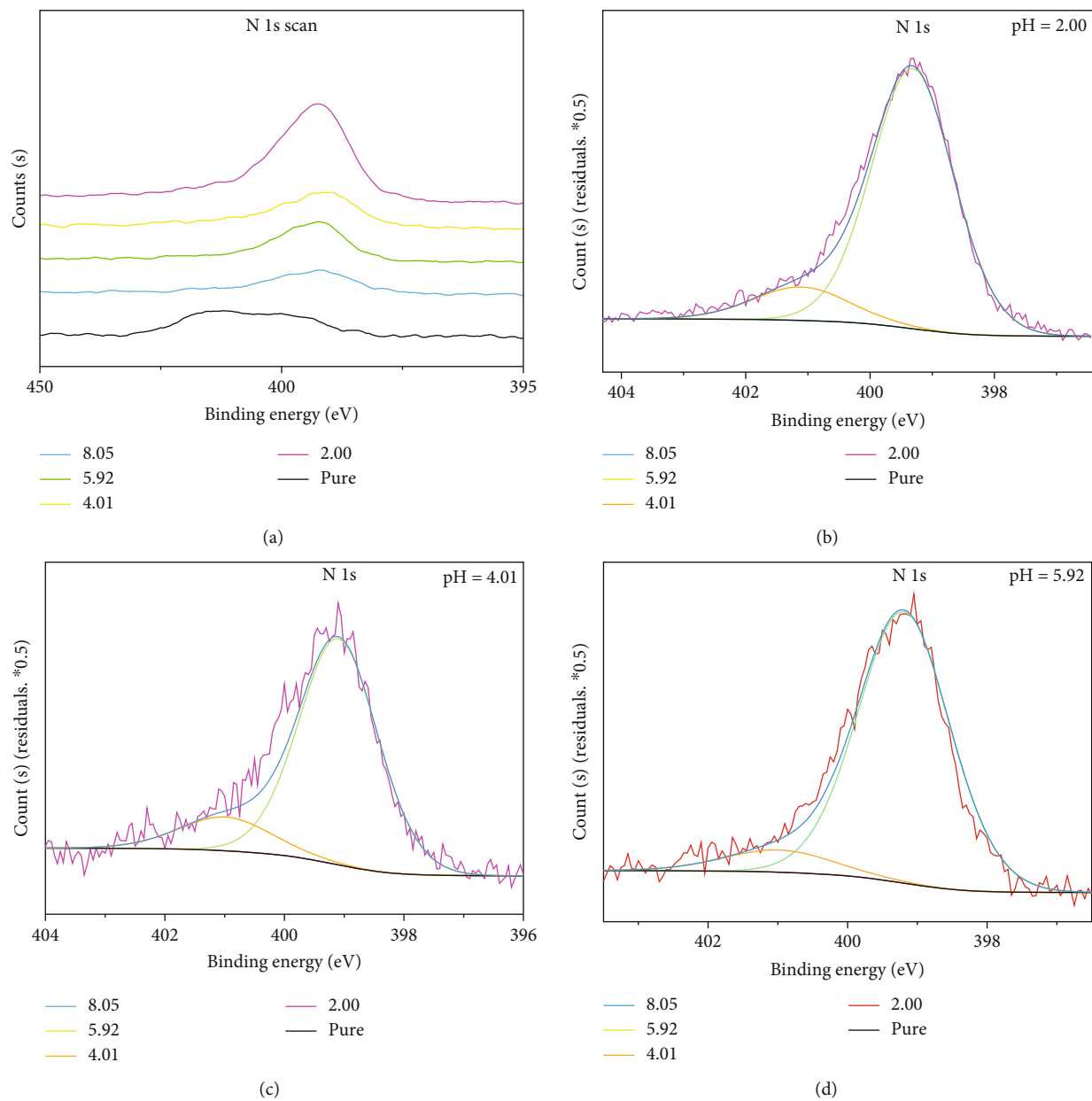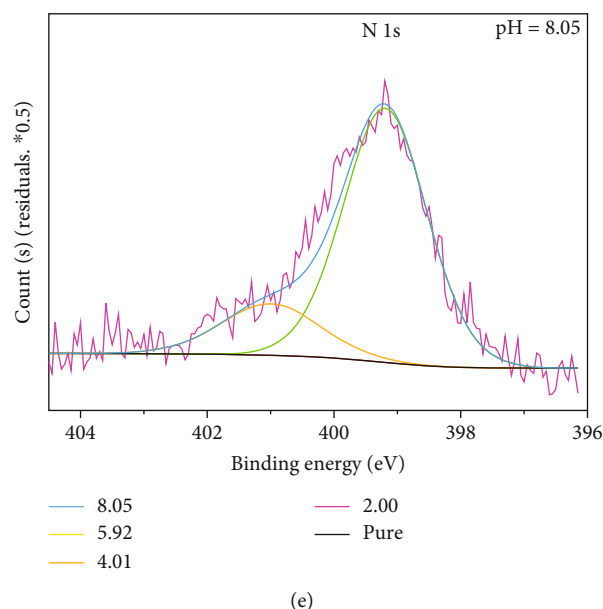
N 1s scan

8.05
5.92
4.01
2.00
Pure

(a)

N 1s   pH = 2.00

8.05
5.92
4.01
2.00
Pure

(b)

N 1s   pH = 4.01

8.05
5.92
4.01
2.00
Pure

(c)

N 1s   pH = 5.92

8.05
5.92
4.01
2.00
Pure

(d)

Figure 7: Continued.

(e)

FIGURE 7: The best fit of the N 1s XPS spectra of acid δ-MnO$_2$ (pure) and δ-MnO$_2$ after reaction with MB at different pH (2.00, 4.01, 5.92, and 8.05).

reaction. As shown in Figure 5, at pH 2.00 and 4.01, δ-MnO$_2$ is accompanied by the release of Mn^{2+} in the process of removing MB. At pH 2.00, the release of Mn^{2+} reaches 13.3 mmol/L. When the pH was 4.01, the release of Mn^{2+} was only 0.76 mmol/L, and the lower the pH, the greater the release of Mn^{2+}. When the pH was 5.92 and 8.05, Mn^{2+} was not detected in the solution after the reaction. However, it can be seen from Figure 3 that the redox reaction still occurs at pH 5.92 and 8.05. It can be inferred that the negative charge on the surface of δ-MnO$_2$ will increase with the pH under weakly acidic, neutral, and alkaline conditions. However, the corresponding adsorption sites that can adsorb positively charged Mn^{2+} increase accordingly; that is, the Mn^{2+} released during the reaction is readsorbed to the surface of δ-MnO$_2$, so Mn^{2+} is not detected in the solution.

4.2. The Mechanism of Adsorption. By comparing the changes of the FTIR spectra of δ-MnO$_2$ before and after the reaction (Figure 6), it was explored whether δ-MnO$_2$ had an adsorption and removal effect on organic matter in the solution. As shown in Figure 6, for the FTIR spectrum of the reacted δ-MnO$_2$, compared with the δ-MnO$_2$ that has not reacted with MB, a new chemical bond vibration is obviously detected. The absorption bands of δ-MnO$_2$ before the reaction are located at 1619, 920, 449, and 512 cm^{-1}, of which 449 and 512 cm^{-1} are the characteristic absorption of δ-MnO$_2$, respectively. The lattice vibration of the layered Mn-O bond has a slight blue shift [29]; 920 cm^{-1} is the bending vibration of manganese-oxygen octahedron-OH [30], and 1619 cm^{-1} is the bending vibration of H$_2$O. After reacting with MB, δ-MnO$_2$ still retains the characteristic peak of δ-MnO$_2$. The layered structure of Mn-O bond lattice vibrates, but the bending vibration of the manganese oxide octahedral cavity -OH at 920 cm^{-1} disappears. At the same

time, many new chemical bond vibrations have appeared. For example, 1395 cm^{-1} was assigned to the stretching vibrations of CN bonds in the heterocycle of MB; the band at about 1491 cm^{-1} was ascribed to the CH$_2$ deformation vibration. In addition, the wave bands at 1252 and 1224 cm^{-1} are due to the Ar-N deformation vibration. For the tensile vibration of C=S and CS, the wave band is about 1142 and 887 cm^{-1}. In the band of 820 cm^{-1}, new chemical bonds appear, which are attributed to the rocking vibration of C-H in the benzene ring of MB [31]. In addition, no bending vibration of -OH at 920 cm^{-1} was detected on the surface of δ-MnO$_2$ after reacting with MB. It can be presumed that the adsorbed material occupied the -OH site of δ-MnO$_2$ and disappeared. It can be seen from Figure 4 that δ-MnO$_2$ is accompanied by the production of intermediate products in the process of removing MB, and the structure of the intermediate product is similar to that of MB. This can prove that the surface of δ-MnO$_2$ adsorbs MB or organic matter similar to MB.

It can also be found from Figure 6 that the adsorbed substances on δ-MnO$_2$ increase with the increase of pH, which is contrary to the result that the adsorption removal rate of δ-MnO$_2$ on MB gradually increases with the increase of pH of the reaction system in Figure 3. Therefore, XPS was used to further quantitatively analyze the content of adsorbed substances on δ-MnO$_2$.

The N element is a characteristic element in the molecular structure of MB and an element that does not exist in the δ-MnO$_2$ structure; for the N element, the δ-MnO$_2$ before and after the reaction is analyzed by XPS (X-ray photoelectron spectroscopy); as shown in Figure 7, XPS analysis found that N element was detected on the reacted δ-MnO$_2$, indicating that the δ-MnO$_2$ had adsorbed the material with N element, and the peak fitting of the N 1s peak of the mineral powder after the reaction was performed (N atoms are not

TABLE 3: The best fit of N 1s XPS spectra for MB adsorption.

	A (pH = 2.00)	A (pH = 4.01)	A (pH = 5.92)	A (pH = 8.05)
N atoms not interacted with acid δ-MnO$_2$ surface	65.95%	69.95%	68.41%	72.32%
The N atoms interacted with acid δ-MnO$_2$ surface	34.05%	30.05%	31.59%	27.68%

A (%): peak area percentage.

directly bonded to the surface of δ-MnO$_2$, and the binding energy of N 1s is 399.2 eV; N atoms are directly bonded to the surface of δ-MnO$_2$, and the binding energy of N 1s is 401.0 eV) [32].

The results are shown in Figure 7(a) and Table 3. As the pH increases, the N content on δ-MnO$_2$ gradually decreases. Under the conditions of pH 2.00, 4.01, 5.92, and 8.05, the ratio of N directly adsorbed on δ-MnO$_2$ to N not directly adsorbed on δ-MnO$_2$ is roughly 1 : 2. It is known that both the structure of MB and its intermediate product contain 3 nitrogen atoms, and the hole -OH on the manganese oxygen octahedron of δ-MnO$_2$ has disappeared. It can be speculated that one N atom in the molecule of the adsorbed substance is adsorbed on the -OH site on the δ-MnO$_2$ hole, while the remaining two N atoms in the molecule do not directly contact the δ-MnO$_2$. Therefore, the δ-MnO$_2$ decolorization MB has an adsorption decolorization process, and the content of adsorbed substances gradually decreases with the increase of pH.

4.3. Removal Mechanism. Based on the above results, it is reasonable to speculate that the removal process of MB by δ-MnO$_2$ is as follows: Under low pH conditions, the δ-MnO$_2$ with a small amount of positive charge on the surface has a high redox potential, so it is strongly oxidizing, and the positively charged MB will be adsorbed on its surface, and then, oxidation reaction occurs. With the consumption of H$^+$ and the release of Mn^{2+}, part of MB is completely degraded into CO$_2$, H$_2$O, and other inorganic substances, and part of it has not been completely degraded. It is accompanied by the generation of intermediate products, including MB parent ion and an MB-analogous compound in which one methyl group is replaced by a proton, Azure B, Azure A, Azure C, Thionin, and other substances.

As the pH of the reaction system increases, the oxidation-reduction potential of δ-MnO$_2$ decreases [17, 33]; the oxidation removal rate of MB decreases significantly with the increase of pH. After the reaction, the UV-Vis band scanning spectrum of the solution can confirm that the oxidation degree of MB gradually decreases with the increase of the pH value. The oxidation of MB by δ-MnO$_2$ is a process that consumes H$^+$, is accompanied by the conversion of high-valence manganese to Mn^{2+}, and is accompanied by the formation of intermediate products. When the initial pH is 2.00, the oxidation removal rate of δ-MnO$_2$ to MB is as high as 98.85%. The more H$^+$ consumed and Mn^{2+} released, the amount of H$^+$ consumed is less than the original system.

As the initial pH increases to 4.01 and 5.53, the oxidation removal rate of MB decreases to 74.49% and 47.43%, and the H$^+$ consumption and Mn^{2+} release in the reaction system gradually decrease. Then, when the initial pH is 7.35, the surface of δ-MnO$_2$ has a large number of negative charges, and the added positively charged dye MB quickly replaces the H$^+$ in the hydroxyl group on δ-MnO$_2$, H$^+$ is released into the solution, so that the H$^+$ in the system increases rapidly, and the pH shows a downward trend. As the oxidation dye reaction progresses, after H$^+$ is gradually consumed, the pH gradually increases, due to the change of pH 7.35 to H$^+$. As the pH of the system increases, the surface of δ-MnO$_2$ becomes electronegative. Through the interaction between charges, Mn^{2+} can be adsorbed to the surface of δ-MnO$_2$, causing the released Mn^{2+} to be readsorbed on the surface of minerals [18, 34], so at high pH, Mn^{2+} is not detected in the system.

The results of FTIR (Figure 6) can prove the adsorption effect of δ-MnO$_2$ on MB. In the experiment, the concentration of the dye after the reaction is measured by using the UV spectrophotometer to measure the absorbance at 664 nm to calculate the concentration of MB. The experiment measured the adsorption and removal of MB by δ-MnO$_2$ as the pH increases. The rate gradually increases, but XPS (Figure 7) shows that under low pH conditions, the number of adsorbed substances is greater. From this, it can be inferred that the adsorbed substances of δ-MnO$_2$ are not only MB. It can be judged by the results of UV-Vis band scanning that MB produced certain intermediate products during the decolorization process, namely, Azure A, Azure B, Azure C, and Thionin. These four intermediate products are obtained by the gradual demethylation of MB. The heterocyclic ring and benzene ring in the MB structure are still undamaged, so the adsorbed substances detected by FTIR and XPS may also include intermediate products in the reaction process, and the molecular weight of these oxidized intermediate products is less than that of MB, which is easier adsorbed on the surface of δ-MnO$_2$. It can be inferred that as the pH of the reaction system increases, the amount of MB adsorbed on the surface of δ-MnO$_2$ gradually increases, but the adsorbed intermediate product decreases.

5. Conclusions

The removal of MB by δ-MnO$_2$ has both oxidation and adsorption mechanisms, and the change of pH significantly affects the oxidation and adsorption of MB by δ-MnO$_2$. We believe that the removal of MB by δ-MnO$_2$ should be divided into two stages: first adsorption and then oxidation. First of all, MB molecules migrate to the vicinity of the mineral surface and then diffuse to the surface of δ-MnO$_2$ through the boundary layer, and adsorbed on the hydroxyl active sites on the surface of δ-MnO$_2$ to replace the H$^+$ in the hydroxyl group, and continue to diffuse into the

micropores inside the adsorbent. Secondly, the adsorbed MB reacts with the high-valence manganese in δ-MnO_2, and the high-valence manganese (Mn^{4+}/Mn^{3+}) is reduced to Mn^{2+}. Part of Mn^{2+} is adsorbed by manganese oxide again due to the Coulomb effect. After the adsorption is saturated, the remaining Mn^{2+} is free in the solution. At the same time, the MB oxidation reaction produces organic intermediate products and some inorganic compounds, and some intermediate products after the MB reaction can also be adsorbed on the surface of δ-MnO_2. Therefore, the research results show that δ-MnO_2 is a combined effect of oxidation and adsorption on the removal of MB.

Data Availability

The data used to support the findings of this study are included within the article.

Conflicts of Interest

The authors declared no potential conflicts of interest with respect to the research, authorship, and/or publication of this article.

Acknowledgments

References

[1] J. E. Post, "Manganese oxide minerals: crystal structures and economic and environmental significance," *Proceedings of the National Academy of Sciences of the United States of America*, vol. 96, pp. 3447–3454, 1999.

[2] S. W. Donne, A. F. Hollenkamp, and B. C. Jones, "Structure, morphology and electrochemical behaviour of manganese oxides prepared by controlled decomposition of permanganate," *Journal of Power Sources*, vol. 195, pp. 367–373, 2010.

[3] T. W. Healy, A. P. Herring, and D. W. Fuerstenau, "The effect of crystal structure on the surface properties of a series of manganese dioxides," *Journal of Colloid & Interface Science*, vol. 21, pp. 435–444, 1966.

[4] J. W. Murray, "The surface chemistry of hydrous manganese dioxide," *Journal of Colloid & Interface Science*, vol. 46, pp. 357–371, 1974.

[5] N. Caliskan, A. R. Kul, S. Alkan, E. G. Sogut, and İ. Alacabey, "Adsorption of zinc(II) on diatomite and manganese-oxide-modified diatomite: a kinetic and equilibrium study," *Journal of Hazardous Materials*, vol. 193, pp. 27–36, 2011.

[6] F. X. Han, Z. L. Mei, T. W. Feng, L. Fan, and H. J. Zheng, "Adsorption and redox reactions of heavy metals on synthesized Mn oxide minerals," *Environmental Pollution*, vol. 147, pp. 366–373, 2007.

[7] W. Tan, F. Liu, X. Feng, Q. Huang, and X. Li, "Adsorption and redox reactions of heavy metals on Fe–Mn nodules from Chinese soils," *Journal of Colloid & Interface Science*, vol. 284, pp. 600–605, 2005.

[8] G. Landrot, M. Ginder-Vogel, K. Livi, J. P. Fitts, and D. L. Sparks, "Chromium(III) oxidation by three poorly crystalline manganese(IV) oxides. 2. Solid phase analyses," *Environmental Science & Technology*, vol. 46, pp. 11601–11609, 2012.

[9] S. Chen, S. Zhang, T. Wang et al., "Structure and properties of vanadium-doped α-MnO_2 and enhanced Pb^{2+} adsorption phenol/photocatalytic degradation," *Materials Chemistry & Physics*, vol. 208, pp. 258–267, 2018.

[10] Y. Wang, B. Q. Han, N. Chen et al., "Beta-MnO_2 microrods for the degradation of methyl orange under acid condition from aqueous solutions," *Research on Chemical Intermediates*, vol. 43, pp. 3975–3987, 2017.

[11] J. Villasenor, P. Reyes, and G. Pecchi, "Catalytic and photocatalytic ozonation of phenol on MnO_2 supported catalysts," *Catalysis Today*, vol. 76, pp. 121–131, 2002.

[12] M. O. Omorogie, J. O. Babalola, E. I. Unuabonah, and J. R. Gong, "Clean technology approach for the competitive binding of toxic metal ions onto MnO_2 nano-bioextractant," *Clean Technologies & Environmental Policy*, vol. 18, pp. 171–184, 2016.

[13] E. J. Elzinga, "Reductive transformation of birnessite by aqueous Mn(II)," *Environmental Science & Technology*, vol. 45, pp. 6366–6372, 2011.

[14] X. Yu, C. Wei, L. Ke, Y. Hu, X. Xie, and H. Wu, "Development of organovermiculite-based adsorbent for removing anionic dye from aqueous solution," *Journal of Hazardous Materials*, vol. 180, pp. 499–507, 2010.

[15] J. Mei and L. Zhang, "Ultrasonic-assisted self-assembly synthesis of highly dispersed b-MnO_2 nano-branches interwoven with graphene flakes for catalytic oxidation of aromatic compounds," *RSC Advances*, vol. 5, pp. 14843–14850, 2015.

[16] P. C. C. Faria, J. J. M. OrfO, and M. F. R. Pereira, "Adsorption of anionic and cationic dyes on activated carbons with different surface chemistries," *Water Research*, vol. 38, pp. 2043–2052, 2004.

[17] M. X. Zhu, Z. Wang, S. H. Xu, and T. Li, "Decolorization of methylene blue by delta-MnO_2-coated montmorillonite complexes: emphasizing redox reactivity of Mn-oxide coatings," *Journal of Hazardous Materials*, vol. 181, pp. 57–64, 2010.

[18] M. X. Wang, P. Pang, L. K. Koopal, G. H. Qiu, Y. Wang, and F. Liu, "One-step synthesis of delta-MnO_2 nanoparticles using ascorbic acid and their scavenging properties to Pb(II), Zn(II) and methylene blue," *Materials Chemistry and Physics*, vol. 148, pp. 1149–1156, 2014.

[19] Y. X. Zhang, X. L. Guo, M. Huang, X. D. Hao, Y. Yuan, and C. Hua, "Engineering birnessite-type MnO_2 nanosheets on fiberglass for pH-dependent degradation of methylene blue," *Journal of Physics and Chemistry of Solids*, vol. 83, pp. 40–46, 2015.

[20] W. H. Kuan, C. Y. Chen, and C. Y. Hu, "Removal of methylene blue from water by gamma-MnO_2," *Water Science and Technology*, vol. 64, pp. 899–903, 2011.

[21] W. H. Kuan and Y. C. Chan, "pH-dependent mechanisms of methylene blue reacting with tunneled manganese oxide pyrolusite," *Journal of Hazardous Materials*, vol. 239, pp. 152–159, 2012.

[22] L. Peng, B. Liu, Q. R. Zeng et al., "Highly efficient removal of methylene blue from aqueous solution by a novel fishing-net

effect of manganese oxide nano-sheets," *Clean Technologies and Environmental Policy*, vol. 19, pp. 269–277, 2017.

[23] R. M. Mckenzie, "The synthesis of birnessite, cryptomelane, and some other oxides and hydroxides of manganese," *Mineralogical Magazine*, vol. 38, pp. 493–502, 1971.

[24] R. M. Mckenzie, "The surface charge on manganese dioxides," *Soil Research*, vol. 19, pp. 41–50, 1981.

[25] H. Kim and N. Saito, "One-pot synthesis of purple benzene-derived MnO_2-carbon hybrids and synergistic enhancement for the removal of cationic dyes," *Scientific Reports*, vol. 8, no. 4342, 2018.

[26] Y. F. Wei, P. Yuan, D. Liu et al., "Activation of natural halloysite nanotubes by introducing lanthanum oxycarbonate nanoparticles via co-calcination for outstanding phosphate removal," *Chemical communications*, vol. 55, pp. 2110–2113, 2019.

[27] Y. F. Wei, X. J. Liang, H. H. Wu, J. M. Cen, and Y. M. Ji, "Efficient phosphate removal by dendrite-like halloysite-zinc oxide nanocomposites prepared via noncovalent hybridization," *Applied Clay Science*, vol. 213, p. 106232, 2021.

[28] M. Zaied, S. Peulon, N. Bellakhal, B. Desmazieres, and A. Chausse, "Studies of N-demethylation oxidative and degradation of methylene blue by thin layers of birnessite electrodeposited onto SnO_2," *Applied Catalysis B-Environmental*, vol. 101, pp. 441–450, 2011.

[29] R. M. Potter and G. R. Rossman, "The manganese-and iron-oxide mineralogy of desert varnish," *Nature*, vol. 25, no. 1-2, pp. 79–94, 1979.

[30] G. Zhao, J. Li, and X. Ren, "Highly active MnO_2 nanosheet synthesis from graphene oxide templates and their application in efficient oxidative degradation of methylene blue," *Rsc Advance*, vol. 3, 2013.

[31] J. Gong, J. Liu, and Z. Jiang, "A facile approach to prepare porous cup-stacked carbon nanotube with high performance in adsorption of methylene blue," *Journal of Colloid and Interface Science*, vol. 445, pp. 195–204, 2015.

[32] L. Y. Zhao, X. K. Wang, Y. G. Guo, N. Z. Wu, and Y. C. Xie, "Adsorption of methylene blue on the muscovite," *Acta Physico-Chimica Sinica*, vol. 10, pp. 896–901, 2003.

[33] H. J. Cui, H. Z. Huang, B. Yuan, and M. L. Fu, "Decolorization of RhB dye by manganese oxides: effect of crystal type and solution pH," *Geochemical Transactions*, vol. 16, p. 10, 2015.

[34] A. Gürses, Ç. Doğar, M. Yalçın, M. Açıkyıldız, R. Bayrak, and S. Karaca, "The adsorption kinetics of the cationic dye, methylene blue, onto clay," *Journal of Hazardous Materials*, vol. 131, pp. 217–228, 2016.